Large Nonstatistical Branching Ratio in the Dissociation of Pentane-2,4-dione Radical Cation: An Ab Initio Direct Classical Trajectory Study

Jia Zhou and H. Bernhard Schlegel*

Department of Chemistry, Wayne State University, Detroit, Michigan 48202

Received: November 17, 2008; Revised Manuscript Received: December 17, 2008

The dissociation of pentane-2,4-dione radical cation has been studied by ab initio direct classical trajectory calculations at the MP2/6-31G(d) level of theory. A bond additivity correction has been used to improve the MP2 potential energy surface (BAC-MP2). A microcanonical ensemble was constructed using quasiclassical normal-mode sampling by distributing 10 kcal/mol of excess energy above ZPE for the transition state for the tautomerization of the enol with a terminal double bond, 4-hydroxypent-4-en-2-one radical cation, to the diketo form. A total of 244 trajectories were run starting from this transition state, yielding pentane-2,4-dione radical cation and depositing energy in the terminal CC bond. As a result, the branching ratio for dissociation of the terminal CC bond versus the interior CC bonds is significantly larger than expected from RRKM theory. The branching ratio for the dissociation of the two interior CC bonds is ~20:1, with the one closest to the activated methyl breaking more often. Since the two interior bonds are equivalent and should dissociate with equal probability, this branching ratio represents a very large deviation from statistical behavior. A simple kinetic scheme has been constructed to model the dissociation rates. The nonstatistical behavior is seen because the rate of energy flow within the molecule is comparable to or less than the rates of dissociation for the activated system. In addition to the expected dissociation products, some of the trajectories also lead to the formation of an ester-like product, prop-1-en-2-yl acetate radical cation.

Introduction

A chemically activated species can dissociate in a nonstatistical manner if the rate for dissociation is faster than the rate for intramolecular energy redistribution. Acetone radical cation is an archetypal example of this process that has been studied experimentally and theoretically over the past 35 years.[1–12] Isomerization from the enol form to the keto form activates the newly formed methyl group, which dissociates preferentially. Energy also flows to the other methyl group, resulting in its dissociation at a smaller rate and with a different energy distribution. The observed branching ratio is ~1.5 in favor of the newly formed methyl group.[1–9,11,12] Similar to acetone radical cation, it can be anticipated that pentane-2,4-dione radical cation will also show nonstatistical behavior in its dissociation. The enol form with a terminal double bond can be generated by the McLafferty rearrangement[13,14] from longer-chain 2,4-diones, as shown in Scheme 1. Upon isomerization to the diketo form, the energy from the activated CC bond can flow sequentially to three other CC bonds, potentially resulting in greater nonstatistical behavior than observed for acetone radical cation.

The formation of pentane-2,4-dione radical cation has been studied experimentally,[15,16] but its dissociation has not been investigated. Similar to our previous studies on acetone radical cation,[11,12] we have used ab initio classical trajectory calculations to study the nonstatistical dissociation of 2,4-pentanedione radical cation. The Born–Oppenheimer molecular dynamics calculations were carried out at the MP2/6-31G(d) level of theory with bond additivity corrections (BACs) fitted to the CBS-APNO energies.

SCHEME 1
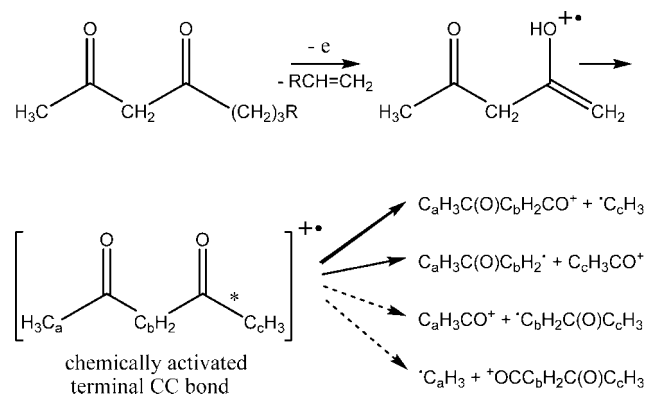
Methods

The Gaussian suite of programs[17] was used for the ab initio electronic structure and molecular dynamics calculations. The geometries of the minima and transition states were optimized by Hartree–Fock (HF), hybrid density functional theory (B3LYP),[18–20] second-order Møller–Plesset perturbation theory (MP2), and quadratic configuration interaction (QCISD)[21] methods. The complete basis set extrapolation methods (CBS-QB3 and CBS-APNO) of Petersson and co-workers[22] were used to compute accurate energy differences. The CBS-APNO calculations have a mean absolute deviation of 0.5 kcal/mol for heats of reaction.

Accurate methods such as CBS-APNO are not practical for molecular dynamics calculations. However, our calculations on the analogous dissociation of acetone radical cation[12] showed that more affordable methods such as density functional theory and MP2 do not yield sufficiently accurate energetics. The errors in such cases are often systematic, arising primarily from the

* Corresponding author. E-mail: hbs@chem.wayne.edu.

making and breaking of bonds. The empirical corrections that have been used to correct computed thermochemistry[23−27] can also be employed to improve potential energy surfaces for molecular dynamics calculations.[28] As in the BAC-MP4 method,[27] a simple exponential is used to correct the potential for bond dissociations. In the present case, the BAC is applied only to the CC bonds for the dissociation of the methyl and acetyl groups (the terminal and interior bonds, respectively):

$$\Delta E = \sum_{i=1}^{2} A_{\mathrm{CC_{interior}}} \exp\left(-\alpha R_{\mathrm{CC_{interior}}}\right) +$$

$$\sum_{i=1}^{2} A_{\mathrm{CC_{terminal}}} \exp\left(-\alpha R_{\mathrm{CC_{terminal}}}\right) \quad (1)$$

The parameters $A_{\mathrm{CC_{interior}}} = 0.0092$, $A_{\mathrm{CC_{terminal}}} = -0.0287$, and $\alpha = 0.3604$ were obtained by fitting the MP2/6-31G(d) energetics to the CBS-APNO level of theory. The structures used in the fit included the diketo isomer, the enol isomer, the diketo−enol transition state, and the methyl and acetyl dissociation products (structures **1**, **7**, **TS8**, **9**, and **10**, respectively; see Figure 1). The corresponding first and second derivatives of ΔE_{BAC} are added to the gradient and Hessian, respectively. This BAC approach has been used previously to study the branching ratios in $\mathrm{CH_2O^{\bullet-}} + \mathrm{CH_3Cl} \rightarrow \mathrm{CH_3CH_2O^{\bullet}} + \mathrm{Cl^-}$, $\mathrm{CH_2O} + \mathrm{CH_3^{\bullet}} + \mathrm{Cl^-}$ [28] and $\mathrm{CH_3COCH_3^{\bullet+}} \rightarrow \mathrm{CH_3CO^+} + \mathrm{CH_3^{\bullet}}$.[11,12]

Ab initio classical trajectories were computed at the BAC-MP2/6-31G(d) level of theory using a Hessian-based predictor−corrector method.[29,30] In this method, a predictor step from the beginning point is taken on the quadratic surface obtained from the energy, gradient, and Hessian. A fifth-order polynomial is then fitted to the energies, gradients, and Hessians at the beginning and end points of the predictor step, and the Bulirsch−Stoer algorithm[31] is used to take a corrector step on this fitted surface with the angular forces projected out. The Hessians are updated for 10 steps before being recalculated analytically. The trajectories were terminated when the centers of mass of the fragments were 8 bohr apart and the gradient between the fragments was less than 1×10^{-5} hartree/bohr. A step size of 0.5 amu$^{1/2}$ bohr was used for integrating the trajectories. The energy was conserved to better than 1×10^{-5} hartree, and the angular momentum was conserved to $1 \times 10^{-8}\hbar$.

Trajectories were initiated at the transition state for the enol-to-diketo tautomerization. A microcanonical ensemble of initial states was constructed using quasiclassical normal mode sampling.[32,33] A total energy of 10 kcal/mol above the zero-point energy (ZPE) of the transition state was distributed among the 38 vibrational modes and the translation along the transition vector toward the product. The total angular momentum was set to zero (corresponding to a rotationally cold distribution), and the phases of the vibrational modes were chosen randomly. The momentum and displacement were scaled to give the desired total energy as the sum of the vibrational kinetic energy and the potential energy obtained from the ab initio surface. The initial conditions were similar to those used previously for acetone radical cation.[11,12] A total of 244 trajectories were integrated for up to 600 fs starting from the transition state and ending when the products were well-separated.

RRKM[34,35] calculations were used to obtain a statistical estimate of the ratio of the dissociation rates for the terminal and interior CC bonds. Variational transition states for bond breaking were approximated by extending the CC bonds and optimizing the remaining coordinates at the BAC-MP2/6-31G(d) level of theory. For the conditions corresponding to the trajectory calculations, the RRKM calculations yielded ratios of 0.10 and 0.11 for terminal versus interior CC bond dissociation at bond extensions of 2.5 and 3.0 Å, respectively.

Results and Discussion

Structures and Energetics. The optimized geometries of the diketo and enol forms of pentanedione radical cation and various intermediates, transition states, and products are shown in Figure 1 for a number of levels of theory. The relative energies of these structures at the CBS-APNO level of theory are included in the figure and are summarized in Figure 2. In its diketo form, pentane-2,4-dione radical cation (**1**) has a planar heavy atom skeleton and belongs to the C_{2v} point group. A second diketo structure, **2**, with the two carbonyl groups syn to the central C−H bonds, lies 6.0 kcal/mol higher. A third conformer, **3**, with one carbonyl syn to a CC bond and the other carbonyl syn to a central C−H bond is 11.5 kcal/mol higher. There are two enolic forms that differ with respect to the location of the C=C double bond. The one with an interior C=C double bond, 4-hydroxypent-3-en-2-one (**4**), is significantly more stable than **1** because of a very strong hydrogen bond between the OH and carbonyl groups as well as conjugation of the C=C and carbonyl double bonds. At lower levels of theory, this structure is symmetrical and has no barrier for proton transfer between the oxygens. At the QCISD/6-311G(d,p) level, the proton-transfer barrier (without ZPE) is 2.5 kcal/mol. Transition state **TS5** for tautomerization from **1** to **4** lies 43 kcal/mol above pentanedione. For the enol isomer with the terminal CC double bond, 4-hydroxypent-4-en-2-one, there are two major conformers to be considered. Conformer **6**, with the OH anti to the C=C double bond, is 11 kcal/mol more stable than the syn conformer **7** because of a strong hydrogen bond between the OH and carbonyl groups. However, it is the syn conformer **7** that is connected to **1** through transition state **TS8**, which is 48 kcal/mol above pentanedione. **TS8** closely resembles the transition state for keto−enol tautomerism in acetone radical cation in both geometry and barrier height.[11,12] The enol-to-diketo tautomerization of **7** via **TS8** to **1** produces a chemically activated pentanedione radical cation that can dissociate into two different sets of products. Breaking the terminal CC bond requires 33 kcal/mol and produces $\mathrm{CH_3C(O)CH_2CO^+} + \mathrm{CH_3^{\bullet}}$ (**9**). Breaking an interior CC bond costs only 27 kcal/mol and produces $\mathrm{CH_3C(O)CH_2^{\bullet}} + \mathrm{CH_3CO^+}$ (**10**). The $\mathrm{CH_3C(O)CH_2CO^+}$ cation has an unusually long CC bond (1.597 Å) that is rather weak (23 kcal/mol). Breaking this bond leads to the triple dissociation product of ketene, acetyl cation, and methyl radical (**11**). The triple dissociation product can also be reached by breaking the CC bond in the $\mathrm{CH_3C(O)CH_2^{\bullet}}$ radical in **10** to yield ketene and methyl radical. The weakness of the CC bonds in pentanedione radical cation can be attributed to the stability of the cationic products $\mathrm{RCH_2CO^+}$, which are isoelectronic to $\mathrm{RCH_2C{\equiv}N}$.

The trajectory calculations revealed a number of additional interesting structures on the pentanedione radical cation potential energy surface. Pentanedione radical cation can rearrange via **TS12** to an ester-like product, $\mathrm{CH_3C(CH_2)OC(O)CH_3}$ (**13**). This product is slightly more stable than **1**, and the transition state is lower than the CC bond dissociation energies of pentanedione radical cation. A second channel revealed by the trajectory calculations involves a proton transfer via **TS14** between $\mathrm{CH_3C(O)CH_2^{\bullet}}$ and $\mathrm{CH_3CO^+}$ before they have separated completely. This produces product complex **15**, which dissociates to the enol of acetone radical cation and ketene, $\mathrm{CH_3C(OH)CH_2^{\bullet+}} + \mathrm{CH_2CO}$ (**16**). **TS14** could be optimized at QCISD/6-311G(d,p) and has an electronic energy 0.4 kcal/mol higher than that of **15**; however, **TS14** could not be located at the MP2
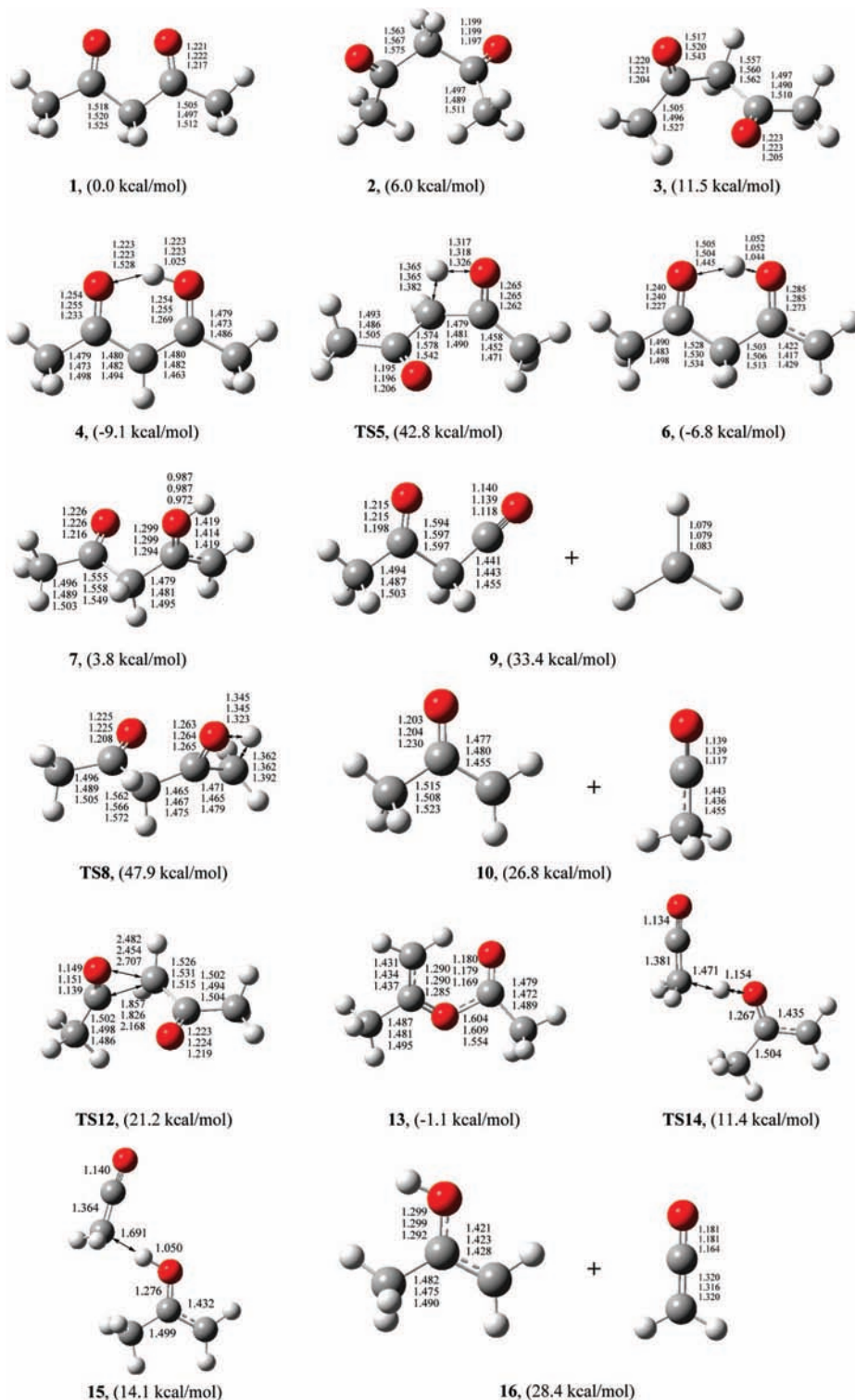
Dissociation of Pentane-2,4-dione Radical Cation

J. Phys. Chem. A, Vol. 113, No. 8, 2009 **1455**

Figure 1. Structures and selected geometric parameters of stationary points on the pentanedione radical cation potential energy surface optimized at the MP2/6-31G(d), BAC-MP2/6-31G(d), and QCISD/6-311G(d,p) levels of theory (top, middle, and bottom rows of values, respectively). For **TS14** and **15**, only the QCISD/6-311G(d,p) values are listed. Bond distances are in angstroms. Relative energies (given in parentheses) were calculated at the CBS-APNO level of theory.

level. When ZPE is included, **15** is higher than **TS14**, suggesting that this feature may be only a shoulder on the potential energy surface.

The relative energies of selected stationary points on the potential energy surface were calculated at a number of levels of theory and are compared in Table 1. The energies were calculated relative to that of **1**, and the CBS-APNO relative energies were taken as reference values in the comparisons. The

CBS-QB3 relative energies agree quite well with the CBS-APNO values, except for the enol isomer **7**. The CBS-QB3 calculations were based on the B3LYP/6-311G(d,p) optimized geometries, while CBS-APNO used QCISD/6-311G(d,p) optimized geometries. B3LYP is relatively poor at predicting the enol geometry, while MP2 and QCISD give similar structures. When the MP2 structure was used for the CBS-QB3 calculation, the relative energy of enol **7** was 4.7 kcal/mol, in better
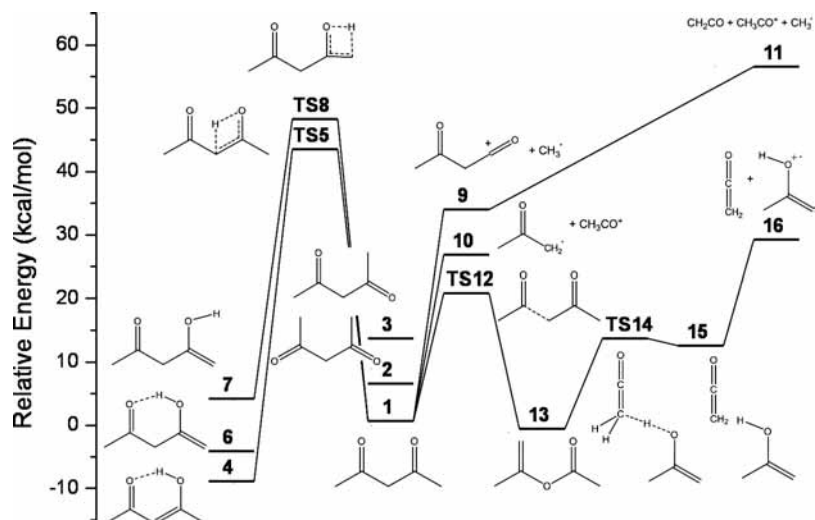
Figure 2. Potential energy profile for the isomerization and dissociation of pentanedione radical cation computed at the CBS-APNO level of theory. For **TS14** and **15**, the relative energies were calculated using QCISD/6-311G(d,p) without ZPE (see the text for details).

TABLE 1: Relative Energies (kcal/mol) of Various Points on the Pentanedione Radical Cation Potential Energy Surface

	HF/ 6-31G(d)	B3LYP/ 6-31G(d)	MP2/ 6-31G(d)	CBS-QB3	CBS-APNO	BAC-MP2/ 6-31G(d)
1	0.0	0.0	0.0	0.0	0.0	0.0
2	14.0	10.2	8.9	9.7	6.0	8.7
3	−9.6	9.9	15.5	14.0	11.5	15.4
4	−24.2	−2.7	−7.2	−8.9	−9.1	−7.4
TS5	42.7	47.1	52.4	44.2	42.8	52.0
6	−20.7	−0.4	−8.1	−6.6	−6.8	−8.6
7	−12.3	8.6	3.5	11.3	3.8	3.0
TS8	45.4	55.4	51.2	50.8	47.9	50.9
9	11.6	43.0	25.0	34.8	33.4	31.4
10	2.2	35.7	27.7	26.9	26.8	25.5
11	33.6	66.6	51.2	56.9	56.6	46.0
TS12	10.5	25.6	19.7	22.0	21.2	19.0
13	−20.8	1.6	−6.2	−0.7	−1.1	−7.7
TS14	0.2	9.5[a]	[b]	12.9	11.4	−1[b]
15	0.2	10.9[a]	[b]	14.1	14.1	−1[b]
16	9.4	34.3	29.3	28.6	28.4	26.4

[a] Obtained using the B3LYP/6-311G(d,p) geometry. [b] Stationary point could not be located (see the text).

TABLE 2: Summary of the ab Initio Molecular Dynamics Calculations for the Dissociation of Pentanedione Radical Cation[a]

product structure	description	branching ratio (%)
10	loss of activated acetyl	43.3
9	loss of activated methyl	29.4
7	enol isomer	18.5
1	diketo isomer	3.8
16	proton transfer	2.1
13	ester-like product	1.6
11	triple dissociation	0.8
10	loss of spectator acetyl	0.4

[a] Based on 238 trajectories integrated at the BAC-MP2/6-31G(d) level of theory starting from the diketo−enol transition state with 10 kcal/mol of excess energy above ZPE in a microcannonical ensemble constructed using quasiclassical normal-mode sampling.

agreement with the CBS-APNO value. The HF calculations greatly overestimate the stabilities of both the enol and ester conformations, while B3LYP underestimates their stabilities compared with the CBS calculations. The barrier height for **7** → **TS8** → **1** is ∼50 kcal/mol at all levels of theory. The CC

SCHEME 2
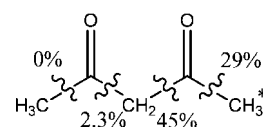
bond dissociation energies (**1** → **9** and **1** → **10**) are ∼20 kcal/ mol too low by HF and 10 kcal/mol too high by B3LYP. A variety of other density functional methods were tested for the dissociation of acetone radical cation, and none was found to provide dramatically superior performance.[12] The MP2 dissociation energy for the interior CC bond is in good agreement with the CBS values, but the dissociation energy of the terminal CC bond is 8−10 kcal/mol too low. The MP2 values with the BAC are in good agreement with the CBS calculations for the two bonds individually. However, the rare event where both bonds break (**1** → **11**) was not included in the calibration of the BAC, and the BAC-MP2 values for that case are ∼10 kcal/ mol too low.

Dynamics. The foregoing discussion has shown that the BAC-MP2/6-31G(d) level of theory is suitable and practical for simulating the molecular dynamics of the pentanedione radical
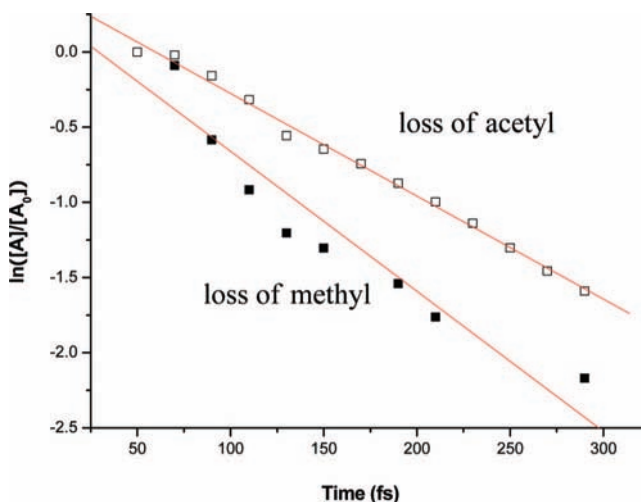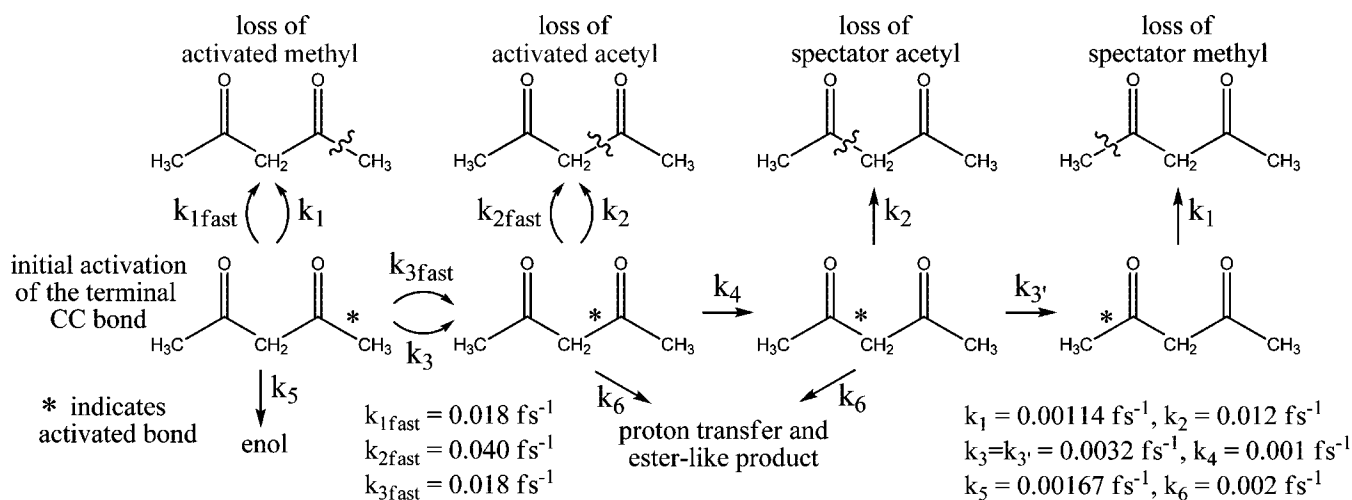

Figure 3. Fraction of undissociated trajectories as a function of time for loss of the activated methyl group (■) and the activated acetyl group (□).

Dissociation of Pentane-2,4-dione Radical Cation

J. Phys. Chem. A, Vol. 113, No. 8, 2009 **1457**

SCHEME 3

cation dissociation. The trajectories were started at the enol-to-diketo transition state, **TS8**. As described in Methods, the initial conditions were chosen from a microcanonical ensemble with 10 kcal/mol of extra energy above the ZPE of the transition state. Of the 244 trajectories that were integrated, six had to be discarded because the energy was not conserved or the integration failed. The distribution of products after excluding these six trajectories is shown in Table 2. There were 44 trajectories that returned to the enol isomer and nine that remained in the diketo minimum. The activated terminal CC bond dissociated in 70 trajectories, producing a methyl radical. The interior CC bond adjacent to the activated terminal CC bond dissociated in 103 trajectories, leading to the loss of an acetyl cation. Only one trajectory produced dissociation of the other interior CC bond. No trajectories showed dissociation of the unactivated terminal CC bond. Two of the trajectories resulted in triple dissociation via **9** by losing first the activated methyl group and then ketene. This fraction is probably too high because the BAC-MP2 energy is 10 kcal/mol too low for this channel. Of the remaining nine trajectories, five yielded the proton-transfer products **16** and four formed the ester-like product **13**.

In acetone radical cation, the two CC bonds have equal bond energies and are expected to dissociate at equal rates. The observed branching ratio of ~1.5:1 thus indicates significant nonstatistical behavior. In pentanedione, the dissociation energy of the interior CC bond is ~6 kcal/mol lower than that of the terminal CC bond. RRKM calculations indicate a ratio of 0.10−0.11 for terminal versus interior CC bond dissociation. Thus, the ratio of 70:103 = 0.68 for terminal versus interior CC bond dissociation obtained from the trajectory calculations represents a significant deviation from statistical behavior. As in the case of acetone radical cation, this is the result of competition between the rate of dissociation and the rate of intramolecular energy flow. An even greater deviation from statistical behavior is seen when the dissociations of the two interior CC bonds are compared. While 103 trajectories produced dissociation of the CC bond adjacent to the activated terminal CC bond, only one trajectory resulted in dissociation of the other interior CC bond. This gives a nonstatistical branching ratio of ~100:1. If the nine trajectories that remained in the pentanedione minimum at the end of the simulation are assumed to dissociate via the interior CC bonds in equal proportions, the branching ratio is ~20:1 (Scheme 2). This represents a very large deviation from statistical behavior, and it is hoped that this result will stimulate some experimental studies.

Some additional understanding of the dissociation behavior of pentanedione radical cation can be obtained by examining

the number of molecules dissociating as a function of time. For the purpose of this analysis, we consider a trajectory to have dissociated when the CC bond length exceeds 3.0 Å and continues to increase. For the 70 trajectories leading to dissociation of the activated terminal CC bond within 600 fs, Figure 3 shows the logarithm of the fraction of undissociated trajectories as a function of time. The corresponding data for the 103 trajectories leading to dissociation of the adjacent interior CC bond are also shown. For unimolecular dissociations obeying first-order kinetics, these plots should be straight lines. In the first ~50 fs, the hydrogen moves from its position in the transition state to form a C−H bond, activating the terminal methyl group but not yet causing any CC bond dissociations. By the end of the next 50 fs, energy has flowed into the terminal CC bond and 50% of the trajectories leading to methyl loss have already dissociated. In contrast, only 20% of the trajectories leading to acetyl loss have dissociated. Energy continues to flow through the molecule, and by 150 fs, 50% of the trajectories leading to acetyl loss have dissociated. Additional time is needed for energy to flow into the other interior CC bond, but the energy also flows into the remaining vibrational coordinates, approaching a statistical distribution and further reducing the dissociation probability. The average dissociation times were 152 fs for the activated methyl group and 205 fs for the activated acetyl group. The dissociation time for the single trajectory leading to loss of the spectator acetyl was ~250 fs.

Figure 3 also shows that the rate constant (i.e., the negative of the slope) for the methyl-group dissociation is larger at earlier times than at later times. The number of methyl groups lost versus time can be fit by two exponentials starting at $t_0 = 60$ fs. The loss of acetyl is also biexponential, but the effect is less pronounced. This suggests that it may be possible to model pentanedione radical cation by assuming that a portion of the population dissociates rapidly, losing the activated methyl and acetyl groups, and that the rest of the population responds more slowly, leading to the remaining products as well as additional methyl and acetyl dissociations. A simple kinetic scheme is given in Scheme 3.

After some testing, we assumed that 40 methyl dissociations and 40 acetyl dissociations arose from the fast mechanism and that the remainder were produced by the slow mechanism. The total number of trajectories leading to each of the products imposed various constraints on the ratios of rate constants. This left four degrees of freedom, which were adjusted to give the best fit to the data shown in Figure 4. Since other kinetic schemes and rate constants may give equally good fits, the
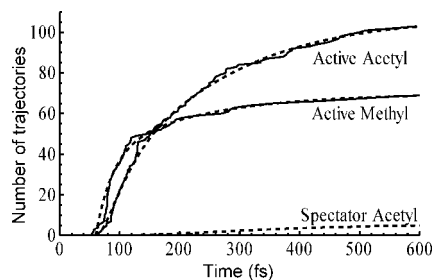
Figure 4. Numbers of dissociations of the activated methyl and acetyl groups as functions of time obtained from the trajectory calculations (solid lines) and from the simple kinetic model (dashed lines).

qualitative relations among the rate constants are more relevant than their numerical values.

Figure 4 shows that the data can be modeled well if one assumes a partitioning of the problem into fast and slow populations. If this assumption is not made, the data at short times (<150 fs) and longer times (>200 fs) cannot both be fit by the same set of rate constants. This suggests that only some of the molecules are highly activated for dissociation by the enol-to-diketo tautomerization. Both the terminal and interior bonds of the highly activated diketo species dissociate rapidly. Energy flows rapidly between the terminal and interior CC bonds, possibly mediated by CCO bending, as suggested by work on the acetone radical cation system.[9,12] The rate constants for the dissociation of the slower population are governed by the behavior at longer times (>200 fs). It is satisfying to note that the ratio of the rate constants for methyl and acetyl dissociation ($k_1/k_2 = 0.095$) is very close to the ratio predicted by the RRKM calculations (0.10−0.11). The rate for energy transfer between the interior CC bonds ($k_4 = 0.001$) is an order of magnitude smaller than the dissociation rate for an interior CC bond. This provides a rationalization for the large non-statistical branching ratio seen for the activated versus spectator acetyl group.

Conclusions

The energetics of pentanedione radical cation dissociation have been studied by electronic structure calculations at a variety of levels of theory up to CBS-APNO. The relative energies calculated at the BAC-MP2/6-31G(d) level gave a better fit to the CBS-APNO results than the MP2 and B3LYP levels of theory. The dissociation of pentanedione radical cation with 10 kcal/mol of extra energy above the diketo−enol transition state has been simulated by ab initio classical trajectories at the BAC-MP2/6-31G(d) level of theory. This dissociation produces pentanedione with chemical activation of a terminal CC bond. Dissociation of this bond yields $CH_3C(O)CH_2CO^+ + CH_3^{\bullet}$, but energy also flows quickly to the adjacent interior CC bond, which dissociates to give $CH_3C(O)CH_2^{\bullet} + CH_3CO^+$. The trajectory calculations also reveal some additional products that were not anticipated. The interior CC bonds are 6 kcal/mol weaker than the terminal CC bonds, and RRKM theory predicts a branching ratio of 0.10−0.11 for terminal versus interior CC bond breaking. However, the simulations yield a branching ratio of 0.68, indicating a substantial deviation from statistical behavior. An even larger deviation from statistical behavior is seen for the dissociation of the two equivalent interior CC bonds, with a branching ratio of ∼20:1 or greater. The biexponential behavior of the dissociations indicates that a fraction of the

activated pentanedione radical cations reacts more rapidly. A simple kinetic scheme has been constructed to model the dissociation rates. The nonstatistical behavior is seen in the dissociations because the rate of energy flow within the molecule is comparable to or less than the rates of dissociation.

References and Notes

(1) Depke, G.; Lifshitz, C.; Schwarz, H.; Tzidony, E. *Angew. Chem., Int. Ed.* **1981**, *20*, 792–793.
(2) McAdoo, D. J.; Hudson, C. E. *Int. J. Mass Spectrom. Ion Processes* **1984**, *59*, 77–83.
(3) McAdoo, D. J.; McLafferty, F. W.; Smith, J. S. *J. Am. Chem. Soc.* **1970**, *92*, 6343–6345.
(4) Turecek, F.; Hanus, V. *Org. Mass Spectom.* **1984**, *19*, 631–638.
(5) Heinrich, N.; Louage, F.; Lifshitz, C.; Schwarz, H. *J. Am. Chem. Soc.* **1988**, *110*, 8183–8192.
(6) Lifshitz, C. *J. Phys. Chem.* **1983**, *87*, 2304–2313.
(7) Lifshitz, C.; Tzidony, E. *Int. J. Mass Spectrom. Ion Phys.* **1981**, *39*, 181–195.
(8) Lifshitz, C.; Tzidony, E.; Terwilliger, D. T.; Hudson, C. E. *Adv. Mass Spectrom.* **1980**, *8A*, 859–866.
(9) Osterheld, T. H.; Brauman, J. I. *J. Am. Chem. Soc.* **1993**, *115*, 10311–10316.
(10) Nummela, J. A.; Carpenter, B. K. *J. Am. Chem. Soc.* **2002**, *124*, 8512–8513.
(11) Anand, S.; Schlegel, H. B. *Phys. Chem. Chem. Phys.* **2004**, *6*, 5166–5171.
(12) Zhou, J.; Schlegel, H. B. *J. Phys. Chem. A* **2008**, *112*, 13121–13127.
(13) Gilpin, J. A.; McLafferty, F. W. *Anal. Chem.* **1957**, *29*, 990–994.
(14) McLafferty, F. W. *Anal. Chem.* **1959**, *31*, 82–87.
(15) Nuzhdin, K. B.; Feldman, V. I.; Kobzarenko, A. V. *J. Phys. Chem. A* **2007**, *111*, 3294–3301.
(16) Hush, N. S.; Livett, M. K.; Peel, J. B.; Willett, G. D. *Aust. J. Chem.* **1987**, *40*, 599–609.
(17) Frisch, M. J.; Trucks, G. W.; Schlegel, H. B.; Scuseria, G. E.; Robb, M. A.; et al. *Gaussian03*, revision F.02; Gaussian, Inc.: Wallingford, CT, 2007.
(18) Becke, A. D. *J. Chem. Phys.* **1993**, *98*, 1372–1377.
(19) Becke, A. D. *J. Chem. Phys.* **1993**, *98*, 5648–5652.
(20) Lee, C.; Yang, W.; Parr, R. D. *Phys. Rev. B* **1988**, *37*, 785–789.
(21) Pople, J. A.; Head-Gordon, M.; Raghavachari, K. *J. Chem. Phys.* **1987**, *87*, 5968–5975.
(22) Montgomery, J. A.; Ochterski, J. W.; Peterson, G. A. *J. Chem. Phys.* **1994**, *101*, 5900–5909.
(23) Allendorf, M. D.; Melius, C. F. *J. Phys. Chem. A* **2005**, *109*, 4939–4949.
(24) Anantharaman, B.; Melius, C. F. *J. Phys. Chem. A* **2005**, *109*, 1734–1747.
(25) Ho, P.; Coltrin, M. E.; Binkley, J. S.; Melius, C. F. *J. Phys. Chem.* **1985**, *89*, 4647–4654.
(26) Melius, C. F.; Allendorf, M. D. *J. Phys. Chem. A* **2000**, *104*, 2168–2177.
(27) Ho, P.; Melius, C. F. *J. Phys. Chem.* **1990**, *94*, 5120–5127.
(28) Li, J.; Shaik, S.; Schlegel, H. B. *J. Phys. Chem. A* **2006**, *110*, 2801–2806.
(29) Bakken, V.; Millam, J. M.; Schlegel, H. B. *J. Chem. Phys.* **1999**, *111*, 8773–8777.
(30) Millam, J. M.; Bakken, V.; Chen, W.; Hase, W. L.; Schlegel, H. B. *J. Chem. Phys.* **1999**, *111*, 3800–3805.
(31) Stoer, J.; Bulirsch, R. *Introduction to Numerical Analysis*; Springer-Verlag: New York, 1980.
(32) Hase, W. L. In *Encyclopedia of Computational Chemistry*; Schleyer, P. v. R., Allinger, N. L., Clark, T., Gasteiger, J., Kollman, P. A., Schaefer, H. F., III, Schreiner, P. R., Eds.; Wiley: Chichester, U.K., 1998; pp 402−407.
(33) Peslherbe, G. H.; Wang, H.; Hase, W. L. *Adv. Chem. Phys.* **1999**, *105*, 171–201.
(34) Marcus, R. A.; Rice, O. K. *J. Phys. Chem.* **1951**, *55*, 894–908.
(35) Steinfeld, J. I.; Francisco, J. S.; Hase, W. L. In *Chemical Kinetics and Dynamics*; Prentice-Hall: Upper Saddle River, NJ, 1999.